CHINA FOUNDRY Research & Development
Vol. 18 No. 5 September 2021
https://doi.org/10.1007/s41230-021-1061-3

Glass formation in Fe-Cr-Zr-B-Mo alloys by tuning Nb addition

Cong-ran Fu[1], Wei Zhang[1], Qing-chun Xiang[1], *Ying-dong Qu[1], Ying-lei Ren[1], Bo Yu[2], **Ke-qiang Qiu[1]

1. School of Materials Science and Engineering, Shenyang University of Technology, Shenyang 110870, China

2. Shenyang Research Institute of Foundry Co. Ltd., Shenyang 110022, China

Abstract: Fe-based bulk metallic glasses (BMGs) with high boron content have potential application as a coating material used in the framework for storing spent nuclear fuels to support their safe long-term disposal. The high glass forming ability (GFA) and large supercooled liquid region are therefore required for such Fe-based BMGs in either the glassy powder fabrication or the subsequent coating spraying. In order to meet these requirements, the influence of Nb content on the GFA of $Fe_{57}Cr_{10}Zr_8B_{18}Mo_{7-x}Nb_x$ (x=1–5, at.%) alloys was investigated, as Nb has positive roles in GFA and thermal stability of BMGs. The results indicate that a fully amorphous phase in the as-cast samples with 3 mm in diameter is obtained for both the $Fe_{57}Cr_{10}Zr_8B_{18}Mo_5Nb_2$ and $Fe_{57}Cr_{10}Zr_8B_{18}Mo_4Nb_3$ alloys. The corresponding supercooled liquid regions of the two BMGs are 78 K and 71 K, respectively. The mechanism for improving their GFA was analyzed based on the principle of metal solidification, the parameters for glass formation and thermal properties of the alloys. The compression strength and Vicker's hardness of the two BMGs are 1,950 MPa and 1,310 HV, 2,062 MPa and 1,180 HV, respectively. The developed BMGs with high B content, good GFA, and very high hardness can be used as coating materials to the framework for spent nuclear fuels.

Key words: amorphous; microstructure; Nb; glass-forming ability; coating material

CLC numbers: TG139$^+$.8 **Document code:** A **Article ID:** 1672-6421(2021)05-450-07

1 Introduction

Fe-based bulk metallic glasses (BMGs) have become the focus of scientific research due to their good soft magnetic properties, excellent mechanical properties, outstanding corrosion resistance, biocompatibility and low material cost [1-4]. In 1995, the first Fe-based BMG with a dimension of millimeters was developed in Fe-Al-Ga-P-C-B system [5]. Subsequently, a series of Fe-based BMGs, such as Fe-Co-(Zr, Hf)-Mo-B-Y [6,7], Fe-Mo-Ga-P-C-B-Si [8], Fe-Cr-Mo-C-B [9], Fe-(Co, Cr, Mn)-Mo-C-B-Y [10-12], Fe-(RE, Nb, Zr)-B [13,14], etc., have been developed. Among them, the Fe-based BMGs containing chromium and molybdenum elements are widely used as coating materials due to their excellent corrosion resistance [15]. Moreover, the Fe-based amorphous coatings with high B content have been considered as promising neutron absorbers for absorbing thermal neutrons in the nuclear industry [16]. To meet the severe service conditions of the coating used in the framework of spent nuclear fuels, Fe-Cr-Mo-B alloy system with both high corrosion resistance and absorbing ability of thermal neutrons may be developed.

It is generally accepted that the amorphous coating made by flame spraying requires the amorphous powder having high glass forming ability (GFA) and large supercooled liquid region. The present Fe-Cr-Mn-Mo-W-B-C-Si [16] alloy system, even with relatively more B content, is not a proper candidate for the coating materials due to its low GFA which will result in the crystallization of the amorphous powder (the precursor of the coating), and inevitably eliminates the advantageous properties of the metallic glasses. Therefore, it is necessary to improve the GFA by tuning the compositions of Fe-based glass-forming alloys.

It is well known that GFA and thermal stability of BMGs are quite sensitive to their compositions. The minor addition has positive roles in the glass formation and thermal stability of BMGs [17]. Nb element has such effects on both Zr-based [18] and Fe-based [19-20] glass forming alloys. It was found that the GFA of

***Ying-dong Qu**

Male, born in 1975, Professor. His research interests mainly focus on carbon fiber reinforced aluminum matrix composites, high entropy alloy and casting new materials.

E-mail: quydong@sut.edu.cn

****Ke-qiang Qiu**

E-mail: kqqiu@sut.edu.cn

Received: 2021-03-29; Accepted: 2021-05-17

$Fe_{70}Zr_{10}B_{20}$ alloy was enhanced by the addition of 4at.% Nb and a fully amorphous rod with a diameter of 1 mm was produced. By adding small amounts of Nb element in Fe-Cr-Mo-C-B alloy system, the $Fe_{46}Cr_{15}Mo_{14}C_{15}B_6Nb_4$ BMG with a diameter of 3 mm was also obtained [20]. However, the B content in these compositions was still lower and the C content was higher, so they are unsuitable for a neutron absorbing material. It was reported that the $Fe_{57}Cr_{10}Zr_8B_{18}Mo_7$ alloy with relatively higher B content and higher GFA was developed, and the glass rods with a diameter of up to 3 mm can be obtained by the copper mold casting method [21]. However, in our experimental conditions, the GFA and the supercooled liquid region of this alloy are not good enough. Therefore, in this work, by tuning the addition amount of Nb, an attempt has been made to develop the new Fe-based BMGs with the compositions of $Fe_{57}Cr_{10}Zr_8B_{18}Mo_{7-x}Nb_x$ (x=1–5) to increase both the GFA and the width of supercooled liquid region, so that the material developed can be applied in the nuclear industry.

2 Experimental procedure

The mixtures of Fe, Cr, Zr, Mo, Nb metal pieces with high purity of 99.2wt.% and Fe-B master alloy (19.35wt.% B) were melted by arc melting in an argon atmosphere to prepare the multicomponent alloy ingots with nominal composition of $Fe_{57}Cr_{10}Zr_8B_{18}Mo_{7-x}Nb_x$ (x=0–5, at.%). For simplicity, the alloy compositions with different Nb additions are expressed as Nb_0, Nb_1, Nb_2, Nb_3, Nb_4, and Nb_5, respectively. The master alloys were re-melted at least four times to obtain the chemical homogeneity. The rod samples with diameters of 2–4 mm and a length of 50 mm were fabricated by the copper mold casting method.

The as-cast samples were examined by the Shimadzu 7000 X-ray diffraction (XRD) with Cu Kα radiation. The thermal stability associated with the glass transition temperature (T_g), onset temperature of crystallization (T_x), supercooled liquid region ($\Delta T_x=T_x-T_g$), and melting behavior was measured by the Netzsch 404F3 differential scanning calorimetry (DSC) at a heating rate of 0.33 $K\cdot s^{-1}$. The microstructure of the as-cast samples was analyzed by the Zeiss Gemini 300 scanning electron microscopy (SEM). To evaluate the mechanical properties of the investigated BMGs, the Vicker's microhardness of cylindrical specimens was measured by the Shimadzu HVS-1000 digital microhardness tester with the loads increasing from 10 to 300 g, at least five samples were measured to ensure that the results are reproducible. The compressive properties of the as-cast BMGs were measured at room temperature by the WDW-100 universal testing machine. The test sample was 2 mm in diameter and 4 mm in length, and the strain rate adopted was 1.0×10^{-4} s^{-1}.

3 Results and discussion

Figure 1 displays the XRD patterns of the as-cast Nb_x (x=0–5) alloy rods with a diameter of 2 mm. All the diffraction patterns consist of two broad peaks in the 2θ region of 40°–50° and 50°–60°, indicating that the microstructure of the as-cast alloys investigated has an amorphous phase. However, the sharp peaks corresponding to the phases of $Fe_{23}B_6$, Fe_3B, Fe_2B and α-Fe are superimposed on the patterns of the as-cast Nb_0, Nb_1, Nb_4 and Nb_5 alloys. Only two of them, i.e., the as-cast Nb_2 and Nb_3 alloy rods, show a fully amorphous nature without the obvious crystalline phases on their patterns. Therefore, it can be concluded that the GFA for Nb_x (x=0, 1, 4, 5) is lower than 2 mm in diameter. The results indicate that the GFA for the Nb-free Nb_0 alloy is lower than that previously reported [21]. The difference in GFA may come from the different purity of the starting materials as well as experimental casting conditions.

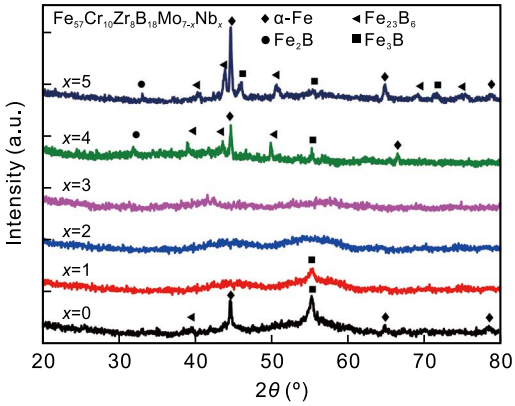

Fig. 1: XRD patterns of as-cast $Fe_{57}Cr_{10}Zr_8B_{18}Mo_{7-x}Nb_x$ (x=0–5) alloy rods with a diameter of 2 mm

To examine the maximum critical diameters of Nb_x (x=2, 3) alloys for their GFA, the alloy rods with diameters of 3 and 4 mm were prepared by increasing the cavity size of the copper molds. The XRD patterns shown in Fig. 2 indicate that the as-cast rods with a diameter of 3 mm for the Nb_x (x=2, 3) alloys are both in amorphous nature while crystalline peaks appear on the patterns of the rods with 4 mm in diameter, showing that the GFA for the Nb_x (x=2, 3) alloys is not larger than 4 mm in diameter. From the intensity of the crystalline peaks embedded on the hump amorphous peaks of samples with 4 mm in diameter, it seems that the GFA for Nb_2 alloy is higher than that of the Nb_3 alloy, which will be further discussed in the following section according to the microstructure analysis.

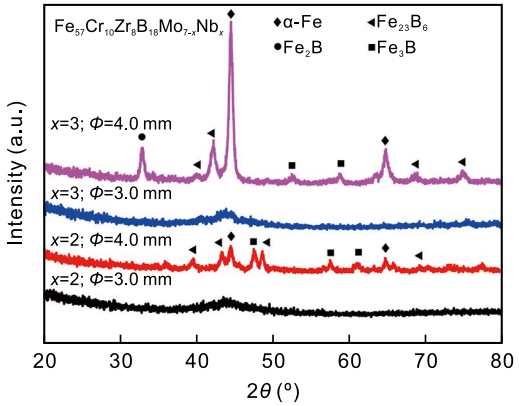

Fig. 2: XRD patterns of as-cast $Fe_{57}Cr_{10}Zr_8B_{18}Mo_5Nb_2$ and $Fe_{57}Cr_{10}Zr_8B_{18}Mo_4Nb_3$ alloy rods with diameters of 3 mm and 4 mm, respectively

Figure 3 shows the SEM images of as-cast Nb_x (x=0–5) alloy rods with a diameter of 2 mm. It can be observed that there is a significant microstructure change with different Nb additions, even if only 1at.% Nb difference exists between two alloy compositions. The microstructure of the as-cast Nb_0 alloy [Fig. 3(a)] consists of countless fine crystalline particles, while for the Nb_1 alloy [Fig. 3(b)], spherical crystalline particles are uniformly distributed in the amorphous matrix. The difference in microstructure indicates that the GFA of the Nb_1 alloy is obviously improved by adding only 1at.% Nb in the Nb_0 alloy. The SEM image of the Nb_2 alloy [Fig. 3(c)] shows a featureless microstructure without any crystalline phases, which indicates that it has an amorphous structure, and is in good agreement with its XRD pattern shown in Fig. 1. With further increasing the Nb addition, as shown in Fig. 3(d), the microstructure of the Nb_3 alloy also exhibits a featureless morphology, which is also consistent with the XRD pattern result shown in Fig. 1. However, in the microstructure of the Nb_4 alloy, there are a lot of white dot and dark crystallites distribute in the amorphous matrix [Fig. 3(e)], indicating that the GFA of the alloy is decreased. When the Nb addition is further increased to 5at.%, the Nb_5 alloy shows a nearly complete crystalline structure [Fig. 3(f)]. Therefore, the better GFA is limited in the alloys with 2at.%–3at.% Nb addition.

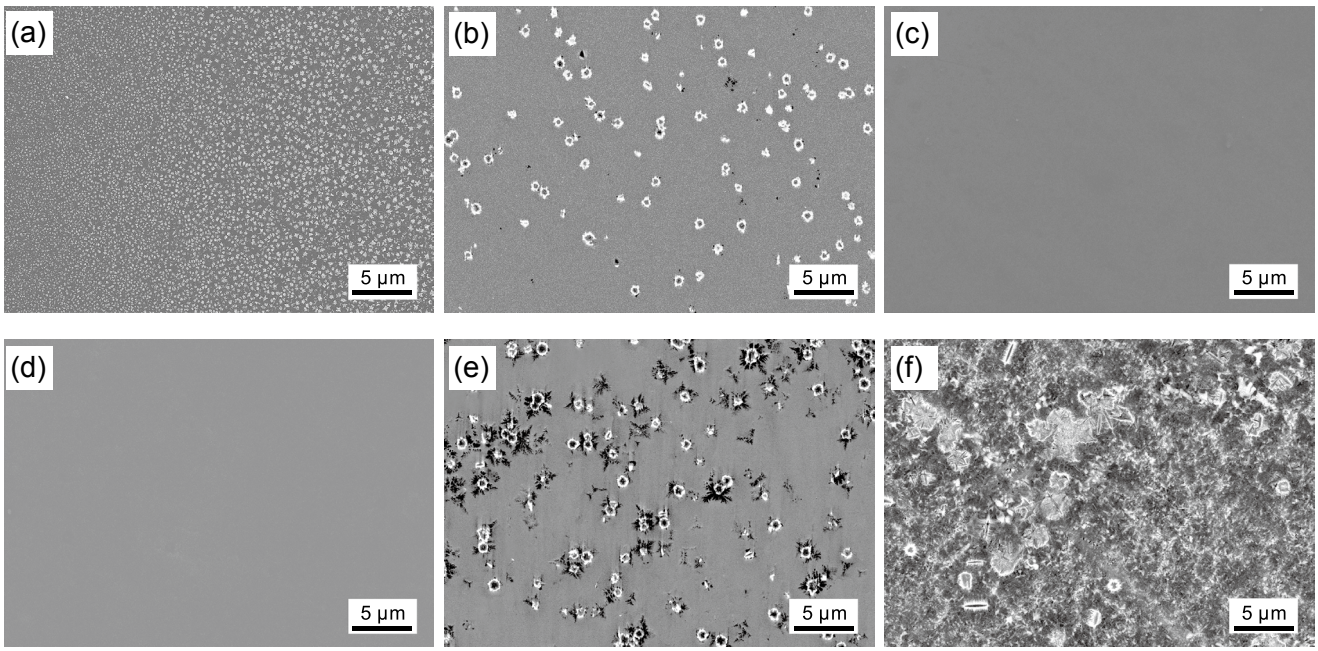

Fig. 3: SEM backscattered images of as-cast $Fe_{57}Cr_{10}Zr_8B_{18}Mo_{7-x}Nb_x$ alloy rods with a diameter of 2 mm: (a) x=0; (b) x=1; (c) x=2; (d) x=3; (e) x=4 and (f) x=5

Figures 4(a) and 4(b) show the SEM images of as-cast rods with a diameter of 3 mm for the Nb_2 and Nb_3 alloys, respectively. It is observed that the Nb_2 alloy [Fig. 4(a)] shows a featureless microstructure without any crystalline phases, indicating that this alloy is in an amorphous structure, corresponding to the XRD pattern shown in Fig. 2. With further increasing the Nb element, a few white dots combined with a very few dark crystallites appear on the SEM image of the Nb_3 alloy [Fig. 4(b)], although no crystalline phases are apparently observed from the XRD pattern shown in Fig. 2. Thus, it is concluded that compared with the Nb_3 alloy, the Nb_2 alloy has better GFA.

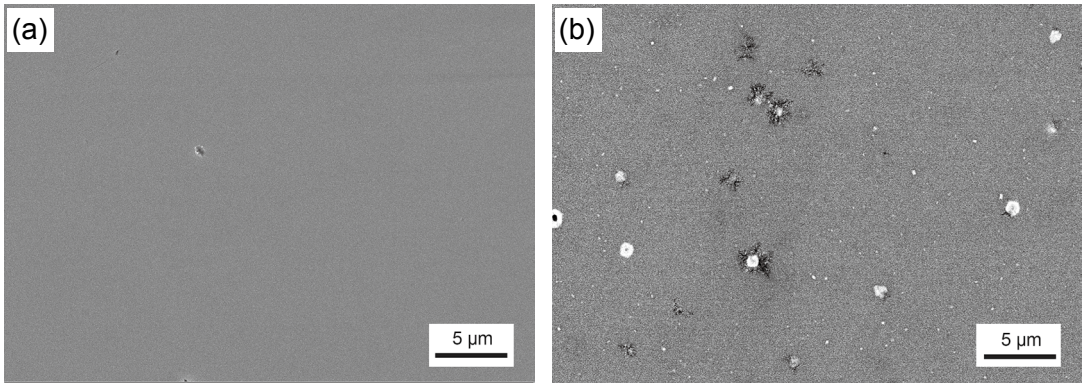

Fig. 4: SEM backscattered images of as-cast alloy rods with a diameter of 3 mm for $Fe_{57}Cr_{10}Zr_8B_{18}Mo_5Nb_2$ (a) and $Fe_{57}Cr_{10}Zr_8B_{18}Mo_4Nb_3$ (b) alloys

Figure 5 shows the DSC curves of the $Fe_{57}Cr_{10}Zr_8B_{18}Mo_{7-x}Nb_x$ (x=1–4) alloy rods with a diameter of 2 mm at a heating rate of 0.33 K·s^{-1}. Table 1 summarizes the glass transition temperature T_g, onset crystallization temperature T_x, onset melting temperature T_m, liquidus temperature T_l (marked by arrows in Fig. 5, respectively), supercooled liquid region ΔT_x (ΔT_x=T_x–T_g), reduced glass transition temperature T_{rg} (T_{rg}=T_g/T_l), as well as the parameter γ [γ=T_x/(T_l+T_g)] [23] which has a close relationship with the GFA of glass-forming alloys [24]. As shown in Fig. 5(a) and Table 1, when the Nb content is increased from 1at.% to 3at.%, ΔT_x firstly increases from 68 K to 78 K, then decreases to 71 K. When the Nb content is further added to 4at.%, it continues to fall to 67 K. It can be seen that the Nb_2 BMG has the largest supercooled liquid region of 78 K, while the supercooled liquid region for the Nb_3 BMG is reduced to ΔT_x=71 K. A larger ΔT_x means that the BMG has a wider temperature range to inhibit crystallization [25], so the Nb_2 BMG has better thermal stability and GFA than the Nb_3 BMG. This is in good agreement with the microstructure observation (Fig. 4). Parameters T_{rg} and γ are often used to characterize the GFA. It can be seen from Table 1 that T_{rg} and γ of the Nb_2 BMG have the largest values of 0.574 and 0.398, respectively, and those of the Nb_3 BMG take the second place. The parameter γ is closely related to the critical cooling rate R_c, and their relationship can be expressed as Eq. (1) [23]:

$$R_c = 5.1\times10^{21}\exp(-117.19\gamma) \quad (1)$$

The high value of the γ indicates a relatively low R_c required for the preparation of amorphous alloys. Therefore, the Nb_2 and Nb_3 alloys have better GFA due to their lower R_c values compared to other alloys.

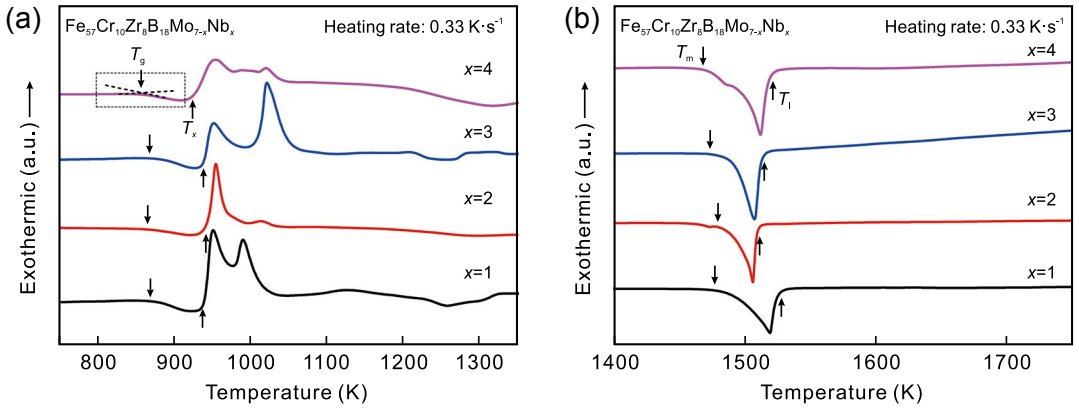

Fig. 5: DSC curves of as-cast $Fe_{57}Cr_{10}Zr_8B_{18}Mo_{7-x}Nb_x$ (x=1–4) alloy rods with a diameter of 2 mm, indicating glass transition and crystallization temperatures (a) and onset and end melting temperatures (b) of alloys

Table 1: Summaries of thermal parameters and mechanical properties of as-cast $Fe_{57}Cr_{10}Zr_8B_{18}Mo_{7-x}Nb_x$ (x=1–4) alloy rods with a diameter of 2 mm (σ_f: compressive fracture strength, HV: hardness)

Alloys	T_g (K)	T_x (K)	T_m (K)	T_l (K)	ΔT_x (K)	T_{rg}	γ	σ_f (MPa)	HV
$Fe_{57}Cr_{10}Zr_8B_{18}Mo_6Nb_1$	869	937	1,476	1,525	68	0.570	0.391	-	1,197
$Fe_{57}Cr_{10}Zr_8B_{18}Mo_5Nb_2$	865	943	1,478	1,505	78	0.574	0.398	1,950	1,310
$Fe_{57}Cr_{10}Zr_8B_{18}Mo_4Nb_3$	867	938	1,472	1,513	71	0.573	0.394	2,062	1,180
$Fe_{57}Cr_{10}Zr_8B_{18}Mo_3Nb_4$	855	922	1,468	1,520	67	0.563	0.388	-	1,010

The GFA of Fe-Cr-Zr-B-Mo-Nb alloys could be further explained with the three empirical criteria proposed by Inoue [26]. Firstly, in this alloy system, the atomic radii of Fe, Cr, Zr, B, Mo and Nb are 0.12412, 0.12491, 0.16025, 0.082, 0.13626 and 0.14290 nm, respectively [27]. The atomic size of the constituent elements increases in the order of B<Fe<Cr<Mo<Nb<Zr. As shown in Fig. 6, the radius of the sphere represents the radius of the alloy atom. Nb with a larger atomic size is used to replace Mo to enhance the mismatch of atomic sizes and improve the stability of liquid phase. Secondly, as shown in Figs. 6(a) and 6(b), the heat of mixing between the Fe-Nb, B-Nb, Fe-Mo, and B-Mo atom pairs is –16, –54, –2 and –34 kJ·mol^{-1}, respectively. The replacement of Mo atom with Nb atom enhances the negative heat of mixing for the main atoms (Fe and B) in the alloy system. The larger negative value of the heat of mixing indicates that there is a strong cohesion and attraction between the constituent atoms, which increases the crystallization resistance of the alloy and improves its GFA [28]. Thirdly, the Nb_2 alloy has the lowest liquidus temperature, which indicates that the composition of the alloy is closer to the eutectic point, and the formation of Fe_3B phase is inhibited by the addition of 2at.% Nb in the alloy. The decrease of liquidus temperature leads to the increase of GFA and thermal stability of the alloy, which is also verified in the Fe-Zr-Co-Al-Mo-B [22] and Fe-Cr-Mo-C-B-Nb [20] alloy systems. It should be noted that the above analysis indicates that the addition of appropriate amount of Nb enhances the GFA of the alloy, but the excessive addition of Nb deteriorates the GFA of the alloy, as shown in Figs. 3(e) and 3(f). This may be

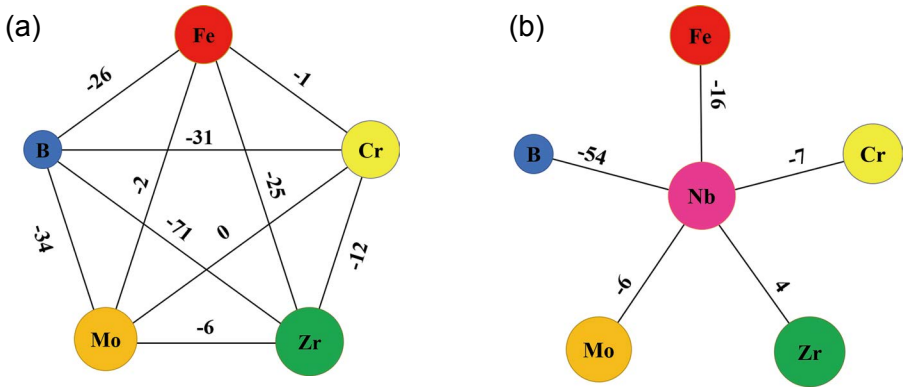

Fig. 6: Schematic diagram of mixing heat for alloy components without (a) and with (b) Nb addition

due to the competition between the configurational entropy of mixing ΔS_{mix} and the enthalpy of mixing ΔH_{mix}, which can be calculated in accordance with Eqs. (2) and (3) [29]:

$$\Delta S_{mix} = -R\sum_{i=1}^{N} c_i \ln c_i \quad (2)$$

$$\Delta H_{mix} = \sum_{i=1, i\neq j}^{N} 4H_{ij}^{mix} c_i c_j \quad (3)$$

where ΔS_{mix} is the configurational entropy of mixing in kJ·mol^{-1}, R the universal gas constant, ΔH_{mix} the enthalpy of mixing in kJ·mol^{-1}, H_{ij}^{mix} the enthalpy of mixing of the binary alloy consisting of element i and j, c_i and c_j are the atomic fractions of element i and j. Figure 7 shows the variation trend of ΔS_{mix} and ΔH_{mix} with the Nb addition in Nb_x (x=0–5) alloys. With the increase of Nb content from 0 to 3at.%, both the values of ΔS_{mix} and negative ΔH_{mix} increases. However, in the competition between the internal energy and the entropy, entropy is dominant and its increase reduces the driving force of crystallization, which means that the alloy has greater GFA. On the contrary, when the Nb addition increases from 4at.% to 5at.%, the internal energy is dominant and the GFA of the alloys becomes poor with the decrease of ΔS_{mix} and the increase of negative ΔH_{mix}. The change tendency of both ΔS_{mix} and the ΔH_{mix} is in good agreement with Figs. 1 and 3.

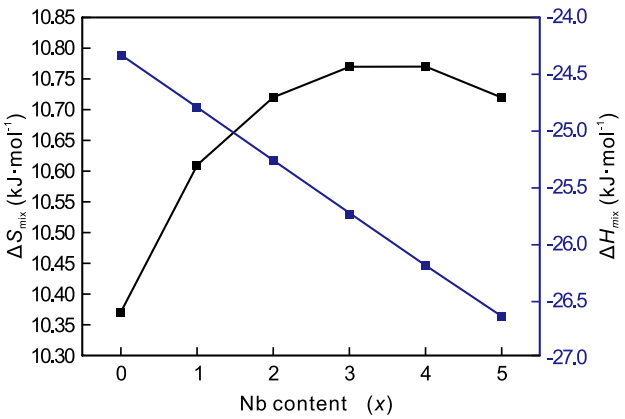

Fig. 7: Varation tendence of configurational entropy of mixing ΔS_{mix} and enthalpy of mixing ΔH_{mix} with Nb addition for $Fe_{57}Cr_{10}Zr_8B_{18}Mo_{7-x}Nb_x$ (x=0–5) alloys

Figure 8 shows the compressive stress-strain curves of the Nb_x (x=2, 3) glassy rods with a diameter of 2 mm at a strain rate of 1×10^{-4} s^{-1}. It can be seen that for the Nb_2 and Nb_3 BMGs, the fracture strengths are up to 1,950 and 2,062 MPa, and the elastic strains are approximately 1.7% and 1.9%, respectively. The high fracture strength of Fe-Cr-Zr-B-Mo-Nb BMGs may correlate with T_g, and the higher the T_g, the better the mechanical properties for Nb_2 and Nb_3 BMGs [30].

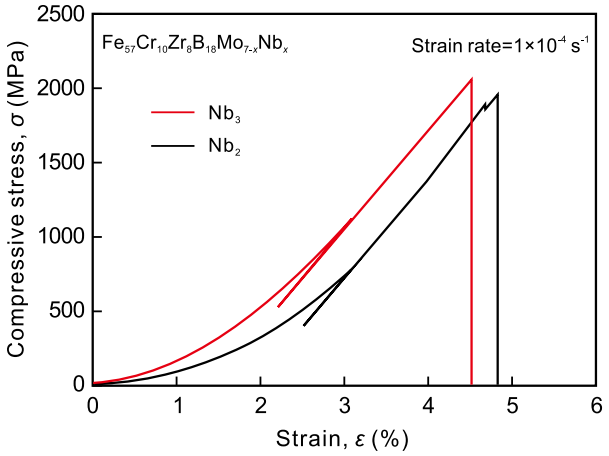

Fig. 8: Strain-stress curves of as-cast $Fe_{57}Cr_{10}Zr_8B_{18}Mo_{7-x}Nb_x$ (x=2, 3) glassy rods with a diameter of 2 mm

The fracture surface images of the Nb_2 and Nb_3 BMG specimens are shown in Figs. 9 and 10, respectively. Figures 9(a) and 10(a) show one of the fragments of the Nb_2 and Nb_3 BMGs after fracture, indicating that both of them exhibit obvious brittle characteristics. As shown in Figs. 9(b) and 10(b), no shear band is observed on the fracture surfaces, indicating that there is no obvious plastic deformation for the Nb_2 and Nb_3 BMGs.

The Vicker's hardness of the Nb_x (x=2, 3) are presented in Table 1. For comparison, Table 2 also summarizes the Vicker's hardness of several typical Fe-based BMGs. It can be seen that among these Fe-based BMGs, the Nb_2 BMG exhibits the highest Vicker's hardness which is up to 1,310 HV. Therefore, it is speculated that the Nb_2 and Nb_3 BMGs have the application potential to be a coating material.

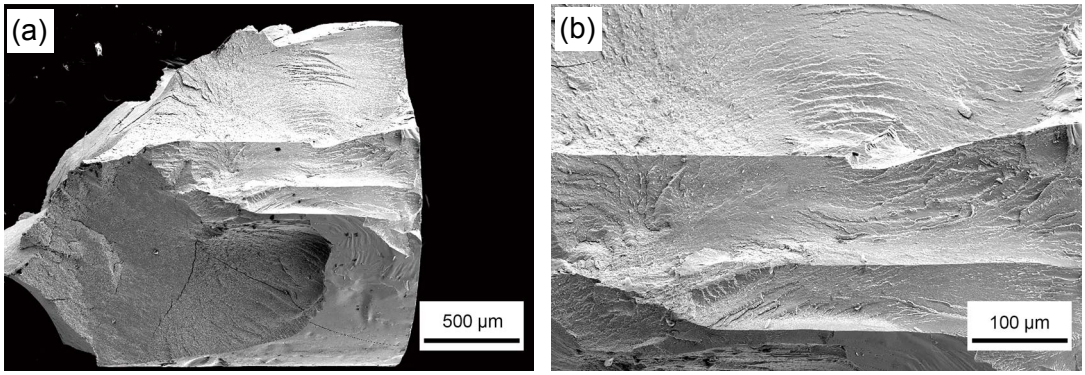

Fig. 9: SEM images of fractured surfaces of $Fe_{57}Cr_{10}Zr_8B_{18}Mo_5Nb_2$ glassy rods with a diameter of 2 mm after compression test: (a) low magnification; (b) high magnification

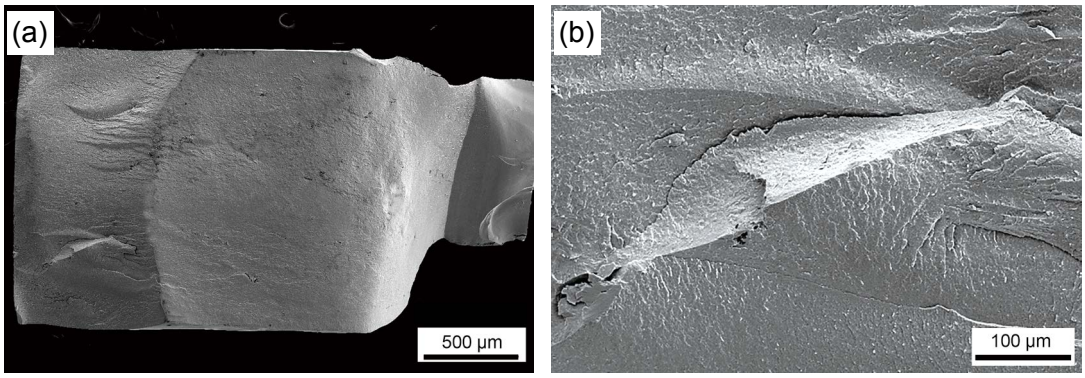

Fig. 10: SEM images of fracture surfaces of $Fe_{57}Cr_{10}Zr_8B_{18}Mo_4Nb_3$ glassy rods with a diameter of 2 mm after compression test: (a) low magnification; (b) high magnification

Table 2: Vicker's hardness of several Fe-based BMGs

Alloys	Hardness	Ref.
$Fe_{50}Cr_{15}Mo_{14}C_{15}B_6$	1,230	[20]
$Fe_{48}Cr_{15}Mo_{14}C_{15}B_6Nb_2$	1,290	[20]
$(Fe_{72}Mo_4B_{24})_{94}Dy_6$	1,130	[24]
$(Fe_{44.3}Cr_5Co_5Mo_{12.8}Mn_{11.2}C_{15.8}B_{5.9})_{98.5}Y_{1.5}$	1,224	[10]
$(Fe_{44.3}Cr_{10}Mo_{13.8}Mn_{11.2}C_{15.8}B_{5.9})_{98.5}Y_{1.5}$	1,287	[10]
$Fe_{48}Cr_{15}Mo_{14}C_{15}B_6Y_2$	1,146	[11]
$Fe_{41}Co_7Cr_{15}Mo_{14}C_{15}B_6Y_2$	1,253	[11]
$Fe_{58}Co_6Ni_4Zr_{10}Mo_5W_2B_{15}$	1,283	[22]
$Fe_{57}Cr_{10}Zr_8B_{18}Mo_5Nb_2$	1,310	This work
$Fe_{57}Cr_{10}Zr_8B_{18}Mo_5Nb_3$	1,180	This work

4 Conclusion

The GFA of $Fe_{57}Cr_{10}Zr_8B_{18}Mo_{7-x}Nb_x$ alloys were investigated, and the best glass former, $Fe_{57}Cr_{10}Zr_8B_{18}Mo_5Nb_2$ alloy with 3 mm in diameter, was identified by the copper mold casting method. The $Fe_{57}Cr_{10}Zr_8B_{18}Mo_5Nb_2$ alloy exhibits the largest supercooled liquid region of 78 K, high compressive fracture strength of 1,950 MPa and Vicker's hardness of 1,310 HV. Comparatively, the GFA of $Fe_{57}Cr_{10}Zr_8B_{18}Mo_4Nb_3$ alloy is almost the same as that of $Fe_{57}Cr_{10}Zr_8B_{18}Mo_5Nb_2$ alloy and exhibits relatively lower supercooled liquid region of 71 K and Vicker's hardness of 1,180 HV, but the highest fracture strength of 2,062 MPa. So, both of $Fe_{57}Cr_{10}Zr_8B_{18}Mo_5Nb_2$ and $Fe_{57}Cr_{10}Zr_8B_{18}Mo_4Nb_3$ alloys have application potential to be a coating material.

Acknowledgements

This work was financially supported by the Liaoning Joint Fund of NSFC (No. U1908219), Natural Science Foundation of Liaoning (No. 2020-KF-14-03) and National Key Research and Development Program of China (No. 2019YFB2006501).

References

[1] Zhai S C, Peng Z R, Guan Y F, et al. Soft magnetic properties and corrosion resistance of Fe-Co-B-M (M, Nb, Ta and NbNi) metallic glasses. Journal of Non-Crystalline Solids, 2019, 506: 28–31.
[2] Liang D D, Wei X S, Chang C T, et al. Effect of W addition on the glass forming ability and mechanical properties of Fe-based metallic glass. Journal of Alloys and Compounds, 2017, 731: 1146–1150.
[3] Li S D, Wei Q, Li Q, et al. Development of Fe-based bulk metallic glasses as potential biomaterials. Materials Science and Engineering: C, 2015, 52: 235–241.
[4] Čukić B, Mitrovic N and Maricic A. Effect of heat treatment on structure and magnetic properties of $Fe_{65.5}Cr_4Mo_4Ga_4P_{12}C_5B_{5.5}$ bulk amorphous alloy. China Foundry, 2017, 14(1): 59–63.
[5] Inoue A, Shinohara Y, Gook J S. Thermal and magnetic properties of bulk Fe-based glassy alloys prepared by copper molding casting. Materials Transactions Jim, 1995, 36: 1427–1433.
[6] Lu Z P, Liu C T, Porter W D. Role of yttrium in glass formation of Fe-based bulk metallic glasses. Applied Physics Letters, 2003, 83(13): 2581–2583.
[7] Guo S F, Wu Z Y, Liu L. Preparation and magnetic properties of FeCoHfMoBY bulk metallic glasses. Journal of Alloys and Compounds, 2009, 468: 54–57.
[8] Shen B, Akiba M, Inoue A. Effects of Si and Mo additions on glass-forming in FeGaPCB bulk glassy alloys with high saturation magnetization. Physical Review B, 2006, 73: 104204.
[9] Pang S J, Zhang T, Asami K, et al. Formation of bulk glassy $Fe_{75-x-y}Cr_xMo_yC_{15}B_{10}$ alloys and their corrosion behavior. Journal of Materials Research, 2002, 17(3): 701–704.
[10] Lu Z P, Liu C T, Thompson J R, et al. Structural amorphous steels. Physical Review Letters, 2004, 92(24): 245503.
[11] Shen J, Chen Q J, Sun J F, et al. Exceptionally high glass-forming ability of an FeCoCrMoCBY alloy. Applied Physics Letter, 2005, 86: 151907.
[12] Ponnambalam V, Poon S J. Fe-based bulk metallic glasses with diameter thickness larger than one centimeter. Journal of Materials Research, 2004, 19(5): 1320–1323.
[13] Lin C Y, Tien H Y, Chin T S. Soft magnetic ternary iron-boron-based bulk metallic glasses. Applied Physics Letter, 2005, 86: 162501.
[14] Yao J H, Yang H, Zhang J, et al. The influence of Nb and Zr on glass-formation ability in the ternary Fe-Nb-B and Fe-Zr-B and quaternary Fe-(Nb,Zr)-B alloy systems. Journal of Materials Research, 2008, 23(2): 392–401.
[15] Branagan D J, Swank W D, Haggard D C, et al. Wear-resistant amorphous and nanocomposite steel coatings. Metallurgical and Materials Transactions: A, 2001, 32(8): 2615–2621.
[16] Farmer J, Choi J S, Saw C, et al. Iron-based amorphous metals: High-performance corrosion-resistant material development. Metallurgical and Materials Transactions: A, 2009, 40(6): 1289–1304.
[17] Wang W H. Roles of minor additions in formation and properties of bulk metallic glasses. Progress in Materials Science, 2007, 52: 540–596.
[18] Johnson C. Synthesis and characterization of particulate reinforced $Zr_{57}Nb_5Al_{10}Cu_{15.4}Ni_{12.6}$ bulk metallic glass composites. Acta Materialia, 1999, 47(8): 2455–2462.
[19] Wang C Y, Li X, Shi Z G, et al. Effect of similar element Nb and Ti substitution for Zr in $Fe_{70}(ZrNbTi)_{10}B_{20}$ bulk metallic glasses. Journal of Non-Crystalline Solids, 2020, 529: 119765.
[20] Zhai F, Pineda E, Duarte M J, et al. Role of Nb in glass formation of Fe-Cr-Mo-C-B-Nb BMGs. Journal of Alloys and Compounds, 2014, 604: 157–163.
[21] Si J, Wu Y, Wang T, et al. Composition-controlled active-passive transition and corrosion behavior of Fe-Cr-(Mo)-Zr-B bulk amorphous steels. Applied Surface Science, 2018, 445: 496–504.
[22] Chen Q J, Fan H B, Ye L, et al. Enhanced glass forming ability of Fe-Co-Zr-Mo-W-B alloys with Ni addition. Material Science and Engineering: A, 2005, 402: 188–192.
[23] Lu Z P, Liu C T. A new glass-forming ability criterion for bulk metallic glasses. Acta Materialia, 2002, 50: 3501–3512.
[24] Tao S, Ma T Y, Jian H, et al. Glass forming ability, magnetic and mechanical properties of $(Fe_{72}Mo_4B_{24})_{100-x}Dy_x$ (x=4–7) bulk metallic glasses. Material Science and Engineering: A, 2010, 528(1): 161–164.
[25] Inoue A, Zhang T, Masumoto T, et al. Glass-forming ability of alloys. Journal of Non-Crystalline Solids, 1993, 156–158: 473–480.
[26] Inoue A. Stabilization of metallic supercooled liquid and bulk amorphous alloys. Acta Materialia, 2000, 48: 279–306.
[27] Senkov O N, Miracle D B. Effect of the atomic size distribution on glass forming ability of amorphous metallic alloys. Materials Research Bulletin, 2001, 36: 2183–2198.
[28] Ponnambalam V, Poon S J, Shiflet G J, et al. Synthesis of iron-based bulk metallic glasses as nonferromagnetic amorphous steel alloys. Applied Physics Letters, 2003, 83(6): 1131–1133.
[29] Guo S, Liu C T. Phase stability in high entropy alloys: Formation of solid-solution phase or amorphous phase. Progress in Natural Science, 2011, 21: 433–446.
[30] Wang W H. Elastic moduli and behaviors of metallic glasses. Journal of Non-Crystalline Solids, 2005, 351: 1481–1485.